CONF-830452--4

MASTER

Paper for presentation at the IAEA Technical Committee Meeting on Non-Inductive Current Drive in Tokamaks, Culham, Abingdon, Oxfordshire, April 18-21, 1983; and for publication in the Proceedings.

CONF-830452--4

DE83 014340

DRIVER OPTIONS AND BURN-CYCLE SELECTION BASED ON POWER-REACTOR CONSIDERATIONS*

David A. Ehst

Fusion Power Program
Argonne National Laboratory
9700 South Cass Avenue
Argonne, Illinois 60439, U.S.A.

Submitted April 1983

DISCLAIMER

*Work supported by the U. S. Department of Energy.

EHB

DRIVER OPTIONS AND BURN-CYCLE SELECTION BASED ON POWER-REACTOR CONSIDERATIONS

David A. Ehst

Fusion Power Program
Argonne National Laboratory
9700 South Cass Avenue
Argonne, Illinois 60439, U.S.A.

Abstract

Reactor implications for noninductive current drive are presented based on a number of studies. First, the lower hybrid driver for the STARFIRE reactor is discussed and the disadvantages of this driver are reviewed. Next, the results of an extensive search for a better current driver are presented. A large number of alternatives were compared in a common context, the DEMO reactor, in order to examine their suitability on a standard basis. Finally, the methodology of a study, currently in progress, is described. The goals of this last study are to compare tokamak reactor designs optimized for operation under different burn cycles, in order to assess the actual benefits and costs of pulsed versus steady-state operation.

1. Motivation for this study - the STARFIRE reactor

The design team which created the STARFIRE reactor concept [1] was strongly influenced by engineering experience and electric utility concerns to select purely continuous (CW) tokamak operation as the preferred mode of operation. This choice was based on intuitive feelings that CW operation would result in a more desirable power reactor compared to one operating in the conventional, ohmically heated (OH) and inductively driven mode. Certain advantages of CW operation were incorporated into the design: (i) by eliminating the Ohmic heating coil (OHC) the central hole in the doughnut was minimized, permitting a relatively compact (seven-meter major radius, R_0) design; (ii) the elimination of thermal fatigue in the first wall and limiter permitted a design at higher thermal wall loads and created the opportunity to utilize a solid breeder compound in the blanket; (iii) the expense of thermal storage associated with cyclic operation was eliminated; (iv) the antitorque structure for the toroidal field coils (TFC) was simplified by eliminating fatigue as a consideration; (v) power supply costs were reduced through the use of very long startup times (20 min) for the current and fusion power ramps; (vi) electric energy storage was eliminated; and (vii) disruptions were assumed to occur less frequently, resulting in less cumulative damage to the first wall and limiter. These features, combined with a perceived higher reliability of a complicated system when operating in a continuous mode, permitted the design of an economically attractive reactor which could approach the high availability goals (75-80%) required for power generation.

The penalty associated with CW operation is due to the circulating power and capital cost of the noninductive driver, and major compromises were made in the STARFIRE design in order to reduce the driver power to a tolerable level [2]. The first major sacrifice was the selection of a rather low plasma density (average electron density $\bar{n}_e = 1.2 \times 10^{20}$ m^{-3}) since this is expected to reduce noninductive current drive power. The drawback was that the fusion power was considerably lower (with $\bar{T}_e = 17$ keV, $\bar{T}_i = 24$ keV) for a fixed beta limit ($\beta_t = 0.067$) and maximum toroidal magnetic field ($B_M = 11.1$ T at the TFC) than it would have been at the optimum density and temperatures ($\bar{n}_e \approx \bar{n}_i \approx 2.4 \times 10^{20}$ m^{-3} and $\bar{T}_e \approx \bar{T}_i \approx 10$ keV). The second major effort was the search for desirable plasma equilibria which exhibit acceptably high stable beta but minimize the total driver power required to sustain the toroidal current, I_0. The latter criterion demands a low current equilibrium with the current density, j, peaked in the region of low electron density, n_e, where noninductive current drive is most efficient. These goals were met with a hollow current density profile with $I_0 = 10.1$ MA. The disadvantage here was that this equilibrium was found to be stable to only modest values of beta.

As a result of these compromises the STARFIRE design appeared to offer a desirable tradeoff between a circulating power and fusion power. It was estimated that CW operation of STARFIRE resulted in a 20% net reduction in the cost of energy compared to that of a comparable power reactor operating in a conventional OH burn cycle. It is difficult to identify other tokamak design improvements which can have such a large influence on the cost of energy! Nevertheless, we are motivated to question whether the situation might be improved by a more judicious choice of current driver than the lower hybrid waves which were selected as the reference driver for STARFIRE. In particular we note that the 10-MA current required driver power absorbed in the plasma at the level $P_d = 67$ MW, with circulating electric power of $P_d^{(e)} = 153$ MW and

correspondingly high capital costs for the driver hardware. In like manner it would seem desirable to identify an alternative to the lower hybrid driver which results in a more credible, centrally peaked current profile which has stability to high beta. With these objectives in mind a survey of noninductive drivers was performed in conjunction with the DEMO reactor study.

2. Comparison of drivers for CW current drive - the DEMO reactor

The DEMO reactor study [3] provided the first opportunity to compare different drivers in a common context. Details of the driver survey can be found in Ref. 4, but the major results will be repeated below. The survey guidelines were as follows. All drivers were required to generate the full toroidal current (I_0 = 9.0 MA) of a high beta ($\bar{\beta}_t$ = 0.08), low safety factor (q_ℓ = 1.9) equilibrium with a centrally peaked current density. Purely steady-state plasma conditions were assumed (i.e., no cycling of density, current, etc.). The toroidal field (B_M = 10.0 T) and tokamak dimensions (R_0 = 5.2 m, aspect ratio, A = 4.0, and elongation, κ = 1.6) were fixed. Temperature and density profiles were fixed ($T = T_0\hat{\psi}^{1.1}$ and $n = n_0\hat{\psi}^{0.3}$, where $\hat{\psi}$ is the normalized poloidal flux [4]), but the average plasma temperatures, $\bar{T}_e$ and $\bar{T}_i$, and densities, $\bar{n}_e$, $\bar{n}_D$, $\bar{n}_T$, . . ., could be varied subject to the fixed $\bar{\beta}_t$ = 0.08 and consistent with a profile-averaged steady-state power balance.

The primary figure of merit in this comparison study is the net electric power produced by the power plant; we computed this in megawatt units as $P_{net} = 0.36 \times P_f - 22 - (P_d/\eta_d)$, where the fusion power, P_f, and P_d are functions of temperature, $\bar{T}_e$, and density. The driver power and the electric-to-driver efficiency, η_d, vary greatly among different drivers, and we caution that our confidence in calculating P_d suffers in many cases from poorly developed current drive theory and a lack of experimental verification of the theories. Likewise, η_d is an estimated quantity for most drivers. Needless to say, our conclusions might change if future developments significantly alter our present understanding of current drive physics or driver system efficiencies.

A secondary consideration in our study is the engineering compatibility of the driver with a tokamak, including reliability and maintenance questions. A final issue, which we cannot neglect, is the estimated capital cost for the driver system.

Driver technology (engineering credibility) has not played a role in the evaluation of alternative drivers. Thus, technology development needs (e.g., for gyrotrons) have not influenced the selection process. Rather, the results of this study may serve the reverse purpose, namely, to indicate which current drive technologies need increased research and development emphasis.

Table I is a catalog of the driver options considered. Our present discussion of most of these is necessarily brief; refer to Ref. 4 for computational details and literature citations for the theoretical and experimental bases of our work.

It is illustrative to first compare the theoretical current density to power density, p, ratio for different drivers, and this is readily done for most of the candidates in the table. This ratio is expressed as

$$j(r)/p(r) = 9.6 \times 10^{17}[20/\ell n\ \Lambda]T_e(r)n_e(r)^{-1}\ \hat{j}/\hat{p}\ ,$$

where $\ell n\ \Lambda$ is the Coulomb logarithm, units are MKS and keV, and the normalized ratio, $\hat{j}/\hat{p}$, is a function of the location in electron parallel velocity space, $v_\parallel$, where the driver power is absorbed. A compendium of $\hat{j}/\hat{p}$ values, computed by many authors, is displayed in Fig. 1; here $v_e \equiv \sqrt{T_e/m_e}$, where m_e is the electron rest mass. Clearly, $\hat{j}/\hat{p}$ is quite sensitive to the local value of $v_\parallel/v_e$, and the premier challenge of noninductive current drive in reactors is to devise a driver system with the optimum $v_\parallel/v_e$ variation throughout the plasma volume. Control of $v_\parallel$ is straightforward for a few drivers, such as neutral beams (NB) and relativistic electron beams (REB). This is not so for many waves; for example, for lower hybrid (LH) waves of frequency $\omega/2\pi$, $v_\parallel = \omega/k_\parallel$, and the parallel wave number, $k_\parallel$, can vary in a complicated manner determined by the plasma dispersion properties. Likewise, it is essential to provide strong absorption of the driver power to achieve substantial current generation. Thus, in the case of the REB, if the driver has difficulty depositing power near the magnetic axis then large current density on axis may not be possible, regardless of how large the j/p ratio is. In a similar manner the fast wave exhibits large $\hat{j}/\hat{p}$ at high phase speeds, but, since Landau and transit time damping diminish exponentially at large $v_\parallel/v_e$, very little current generation might result, the wave's power being wasted by ion damping or absorption in the reactor's first wall structure.

Evidently each driver must be examined separately in order to arrange parameters to minimize its total driver power. This has been done in a manner consistent with the appropriate absorption physics and geometric constraints of the DEMO reactor (albeit with varying degrees of rigor, depending on the sophistication of the particular current drive theory). We highlight the three most promising candidates in the next subsection, and thereafter we comment on the others only briefly.

2.1 Most promising drivers

2.1.1 Compressional Alfven wave (CAW)

This CAW is the fast wave branch and exists as a cavity eigenmode at low frequencies ($\omega < \Omega_i$, where Ω_i is the ion gyrofrequency). The toroidal phase speed is determined by an approximate global dispersion relation [5]; by selecting the lowest order perpendicular mode structure and a toroidal mode number $k_\parallel = 20/(R_0)$ the ratio $w \equiv v_\parallel/v_e = \omega/(k_\parallel v_e)$ is minimized while keeping $v_\parallel/v_i$ large enough to avoid ion Landau damping. We find $\omega/2\pi = 5.3$ MHz, and the radial variation of w, given by $T_e(r)$, is displayed in Fig. 2. Provided damping occurs in the linear regime, transit time magnetic pumping (TTMP) results in very efficient current drive; the fast wave curve in Fig. 1 is fitted by $\hat{j}/\hat{p} = 5 + 13/w$ for $w < 1$. Assuming electron TTMP is the sole damping mechanism the radial damping profile is [6]

$$p(r) \propto n_e(r)T_e(r)w\ \exp(w^2/2)b_\parallel^2\ ,$$

where $b_\parallel$ is the wave's magnetic field. If, for the sake of illustration, we take $b_\parallel(r) = $ constant these equations may be combined to yield the current density profile, $j(r)$, shown in Fig. 2. If $b_\parallel(r)$ is centrally peaked then

$\hat{j}(r)$ would have a narrower profile. If we use $\hat{j}(r)$ of Fig. 2 and set the integral of $\hat{j}(r)$ equal to I_0 we find $I_0/P_{CAW} = 0.48\ \bar{T}_{e10}\bar{n}_{e20}^{-1}$ A/W, where $\bar{T}_{e10}$ is in units of 10 keV and $\bar{n}_{e20}$ is in units of 1×10^{20} m^{-3}. Figure 3 shows the net power for a CAW-driven DEMO, assuming an electric efficiency $\eta_{CAW} = 0.7$.

However, this favorable result may be deceiving. Since the CAW is resonant with trapped electrons ($w < 1$), these momentum recipients are not free to circulate toroidally, so it is unclear how large a toroidal current can actually be generated. Fokker-Planck calculations were done in Ref. 7 for Landau damping on trapped electrons. The result for an inverse aspect ratio $\varepsilon \equiv A^{-1} = 0.1$ is included in Fig. 1 and labelled LD. It is apparent that $\hat{j}/\hat{p}$ vanishes as $w \to 0$. If this calculation accurately models toroidal effects then the CAW is not nearly as attractive as Fig. 3 suggests. Nevertheless, the input of canonical angular momentum to the trapped electrons forces their banana centers inwards, towards the magnetic axis, analogous to the Ware pinch. This effectively fuels the central plasma region, creating a density gradient. Fisch and Karney [5] then invoke the bootstrap effect to create toroidal current. However, since electrons do not appear to behave neoclassically in tokamaks, we do not have a lot of confidence in our conclusions regarding CAW-driven currents. Thus, the P_{net} curve in Fig. 3 is left dashed as a reminder of our inability to quantify neoclassical effects.

2.1.2 High phase speed magnetosonic wave (HSMS)

This high frequency ($\omega > \Omega_1$) version of the fast wave is damped by TTMP and thus exhibits relatively large $\hat{j}/\hat{p}$ compared to the slow wave (LH) at phase speeds of interest ($w \gtrsim 1$), as shown in Fig. 1 [5]. Also in contrast to the slow wave, the plasma dispersion properties do not prevent propagation to high central plasma densities at high phase speeds ($n_\parallel \approx 1$). However, attempts to drive currents at large w, where $\hat{j}/\hat{p}$ is largest, may be thwarted by the very weak electron damping in this part of phase space. In particular, ion cyclotron damping will compete strongly with electron damping, tending to reduce the overall current drive efficiency. Two conceptual solutions to this problem are envisoned. The first alternative would require a tokamak design with $A \gtrsim 5$, which eliminates all ion cyclotron damping [8]. In this case relatively large w can be utilized with electron damping achieved via multipass absorption of the HSMS wave. (Of course, losses due to wall reflection or leakage through ports in the torus must also be minimized). The second approach, described below, selects $w \approx 1$ so that strong, single pass electron damping occurs; careful launcher design permits the HSMS rays to pass only through plasma regions which are devoid of ion cyclotron resonances.

Figure 4 shows typical HSMS ray trajectories for an equivalent circular plasma centered on the DEMO's magnetic axis (5.5 m), where $B_{axis} = 4.6$ T. The ion cyclotron resonances are shown for fuel and impurity species. The three-quarter wavelength antenna ($\omega/2\pi = 82$ MHz) of length 95 cm has been located to avoid ray passage through the cyclotron resonances. From each of three initial launch positions we display the evolution of five rays typical of a broad poloidal mode structure, $m = 0, \pm4$, and ±15. Properly constructed, the antenna should excite a narrow spectrum for $k_\parallel = N/R_0$. For $N = 42$ (Fig. 4) we find $k_\parallel$ varies from ~5 m^{-1} to ~9 m^{-1} as the waves traverse the plasma volume. Over the bulk of the plasma $w \approx 1$-2 so electron damping is strong; hash marks indicate 5% power decrements along the rays in Fig. 4. Taking $\hat{j}/\hat{p} \approx 17$ for w near unity, the current density profile was calculated from the radial pro-

files of $n_e(r)$, $T_e(r)$, and $p(r)$. The result for $\bar{T}_e = 16$ keV is shown in Fig. 5.

Numerically integrating $p(r)$ and $j(r)$ we find $I_0/P_{HSMS} = 0.051\ T_{e10}\bar{n}_{e20}$ A/W. The net power production, assuming $\eta_{HSMS} = 0.7$, is the curve labelled "fast wave" in Fig. 3. $P_{net} > 100$ MW and is probably adequate for the DEMO goals. However, even at the lowest densities (highest $\bar{T}_e$) the driver power is very large; $P_{HSMS} = 95$ MW at $\bar{T}_e = 17$ keV. Consequently the driver capital cost is also very large.

The HSMS wave has several advantages. The $j(r)$ profile is centrally peaked. Supposedly the detailed shape of $j(r)$ might be controlled by careful design of the antenna's power spectrum. In addition, provided w is sufficiently large, neoclassical electron trapping should not be significant. The rf technology is similar to the CAW driver system, but the higher frequencies may permit the design of launchers which are essentially re-entrant waveguides, flush with the reactor's first wall [8].

2.1.3 Pulsed relativistic electron beam (REB)

Pulsed injection of relativistic electron beams appears to be another potentially good means of driving toroidal current. In this scheme the REB is injected long enough (~1 μs) to establish a circulating relativistic electron current which exceeds the initial plasma current. The reverse emf cancels most of the REB contribution, but a small increase, ΔI, in the total current occurs. After a period $\Delta t = (L/R)(\Delta I/I)$, determined by the plasma inductance and resistance, the pulse must be repeated. The increase ΔI depends crucially on the dc resistivity of the plasma return current. If R remains neoclassical at all times then the time-averaged power required for the REB is identical with that for CW current drive in the relativistic limit, and the efficiency is no better than that of the lower-hybrid wave; see Fig. 1 with no resistivity enhancement, $\alpha = 1$. However, REB injection appears to drive phase space instability which in turn may greatly increase the resistivity of the plasma return current. In this case, ΔI will be much larger, Δt will be increased, and, for a given REB energy in a pulse, $\mathscr{E}_b$, the average power $P_{av} = \mathscr{E}_b/\Delta t$, will be decreased. If the resistivity exceeds neoclassical by a factor of $\sim 10^3$ the limiting case occurs; then the REB loses negligible energy via Coulomb collisions and instead transfers all its energy to the increased plasma current, viz $\mathscr{E}_b = \Delta I/2(LI^2) = LI\Delta I$. At this point the energy $\mathscr{E}_b$ is stored inductively in the poloidal fields, and hereafter a forward emf drives the current "ohmically". So, in this limit the average power approaches the ohmic heating value: $P_{av} = \mathscr{E}_b RI[L(\mathscr{E}_b/LI)] = I^2R$. Figure 6 displays the results of a more detailed calculation [4] for DEMO assuming the resistivity is enhanced by a factor $\alpha > 10^3$ during the REB lifetime. If the return current's resistivity is not enhanced by such a large factor (e.g., if streaming instabilities are not excited) the reverse emf will be weaker and more of the REB momentum is wastefully dissipated against the plasma ions. In such a case Fig. 6 would underestimate the average power requirement.

The time-averaged $\hat{j}/\hat{p}$ is shown in Fig. 1 for the two extremes, $\alpha = 1$ and $\alpha \gg 1$. Figure 3 shows P_{net} for the DEMO, assuming $\alpha \gg 1$. Notice, since $P_{REB} = I_0^2 R \ll P_f$, the net power is quite close to the gross electric power output, $0.36 \times P_f$. Consequently, P_{net} is insensitive to η_{REB}, the power efficiency of the driver system. The DEMO would require a relativistic $\gamma = 4$

(1.5 MeV) beam delivering 4 MJ to the plasma every 1.5 s. The REB is launched from a plasma diode [9] at the end of a magnetically insulated transmission line (MITL). The bulk of the power conditioning system is in a separate building and consists of motor-driven rotary flux compressors, a high voltage transformer, and a water capacitor which feeds the MITL.

The REB driver is attractive for a number of reasons. It promises low circulating power with small capital costs in a system which seems compatible with the fusion experiment. The MITL may be readily routed around corners to simplify reactor maintenance, and the power train, under development for inertial fusion, is likely to provide reliable operation.

The REB has been demonstrated to provide the full toroidal current (~20 kA) for a short period (~10 ms) in a small, high density ($\sim 10^{20}$ m^{-3}) tokamak with a single pulse injected into a plasma gun target [10]; no transformer was present in the experiments. While the REB thus can unquestionably initiate noninductive toroidal currents, it is not certain if the REB can maintain I_0 for long periods with repetitive injection. The issue here is whether the relativistic electrons can penetrate to the magnetic axis before losing their kinetic energy, in order to provide a centrally peaked current density. The major experiment (on Macrotor) [11] which tested REB injection into an equilibrium with pre-existing toroidal current found current increases, ΔI, in close agreement with the zero-dimensional theory [4], but the spatial profile of REB generated current remains an open question. The P_{net} curves for the REB in Fig. 3 are dashed as an acknowledgment of the uncertainty of the spatial profile for REB-driven currents.

2.2 Less attractive drivers

Here we mention the other alternatives to the LH driver in roughly the order given in Table I. The discussion is mostly qualitative and is aimed toward emphasizing the perceived disadvantages of these drivers found in the more detailed survey of Ref. 4.

- Neutral beam - Numerical calculations showed centrally peaked current density is achievable with $I_0/P_{NB} = 0.065\ \bar{T}_{e10}\bar{n}_{e20}^{-1}$ A/W. As shown in Fig. 3 this might be of interest, but P_{net} is very sensitive to the driver efficiency, η_{NB}. A practical driver would require beams in the MeV range with tens of amperes of negative ions electrostatically accelerated and neutralized by laser photodetachment in order to achieve $\eta_{NB} \approx 0.8$. The main drawback to this driver is the sheer size of the injectors, which limits access to the tokamak, rendering reactor maintenance difficult.

- Partially stripped heavy ions - Charged particle transport through the strong tokamak magnetic fields appears difficult, and this is compounded by the need to ionize and capture the beam near the inboard (high field) region of the plasma. Numerical calculations showed the impracticality of injecting toroidal momentum if centrally peaked power deposition is required.

- Intense pulsed ion beam - Recently developed sources such as the reflex triode and reflex tetrode generate charge-neutral plasma beams with MeV ions and megampere particle currents. Repetitive pulsed injection might sustain the toroidal current, but collisional momentum transfer may dominate the particle dynamics, reducing $\hat{j}/\hat{p}$ to that associated with NB injection. In addition, the beam trapping mechanisms are poorly understood at present.

• Bootstrap - Theoretically this mechanism should produce hollow current densities and so does not fit the DEMO requirements. Experimentally, the evidence for a bootstrap current was clearly absent from the ISX-B data, despite the fact that $\beta_p \gtrsim \sqrt{A}$ was achieved on that device. This may not be surprising since the bootstrap effect relies on neoclassical transport, and tokamaks do not exhibit neoclassical electron behavior.

• Preferential loss of fusion alpha particles - Alpha particle collisionless orbits become better confined as the product $I_0 A$ increases. Unfortunately, this product is so large for DEMO that the toroidal flow anisotropy is very small. In addition, electrons pushed by the alphas reduce the net current, resulting in only ~30 A of current due to this process.

• Shear Alfven wave and ion cyclotron wave - These are the slow wave branches at $\omega \ll \Omega_i$ and $\omega \lesssim \Omega_i$, respectively. Since these waves are electrostatic the $\hat{j}/\hat{p}$ values are smaller than the values obtained for the fast wave, which benefits from the TTMP mechanism.

• Low phase speed magnetosonic wave - This electromagnetic fast wave can be damped principally by TTMP provided $\omega \gtrsim 5\ \Omega_i$. By selecting a large $k_\parallel$ it is possible in principle to generate currents in the desirable range $w \lesssim 1$. However, at these short parallel wavelengths ($\lambda_\parallel \approx 8$ cm) it appears virtually impossible to excite the single mode which generates centrally peaked current density. Instead, surface damping and hollow current density is expected.

• Minority ion cyclotron resonance heating (ICRH) - A ^{3}He minority appears to give the best results, and ray tracing calculations of fast wave damping were done to determine the optimum frequency range and spectrum for current drive. When wave heating occurs at $(\omega - \Omega_{He})/(k_\parallel v_{He}) \approx 6.7$ then $\hat{j}/\hat{p}$ has a maximum of 13.7 (see Fig. 1). However, even in the best case considerable damping occurs away from the maximum of $\hat{j}/\hat{p}$, effectively reducing $\hat{j}/\hat{p}$ to values much less than those obtainable with NB injection. Moreover, neoclassical electron trapping may further reduce $\hat{j}/\hat{p}$; it is even conceivable that regions of reversed current density may appear. Altogether, ICRH prospects for current drive are relatively unattractive.

• Alpha particle wave damping - In principle Landau damping and TTMP can selectively interact with fusion alphas to generate an asymmetric distribution and thereby a circulating minority beam. In order to avoid majority cyclotron damping a frequency $\omega \gtrsim 5\ \Omega_i$ must be used, but it appears difficult to generate centrally peaked current density at these frequencies. As with ICRH, regions of reversed current density may even appear.

• Electron cyclotron resonance heating (ECRH) - ECRH theoretically yields $\hat{j}/\hat{p}$ about 75% of the LH value since the momentum input by the wave is negligible; see Fig. 1 in the linear regime ($D \to 0$). If heating is sufficiently intense ($D \to \infty$) the efficiency equals that of the LH driver. Large $\hat{j}/\hat{p}$ values require $(\omega - \Omega_e)/k_\parallel v_e$ in the range 4-5, but it may be very demanding to design ECRH launchers which direct rays at the exacting angles needed to assure damping in this region of phase space. In fact, if rays should pass through the resonance then bi-directional current density will result. An additional question is the likelihood of developing low cost ECRH sources at acceptably high efficiencies.

• Anisotropic synchrotron radiation reflection - The main drawback of this approach is the low electron temperature of DEMO. Even at a central value T_{e0} = 33.6 keV ($\bar{T}_e$ = 16 keV) we expect currents much less than a megampere to occur. Moreover, maintenance of the appropriate reflectivity of the first wall appears problemmatical in light of wall erosion due to sputtering and disruptions.

3. Burn cycle selection

The purpose of this companion study is to gauge the benefits and costs of reactor operation under different burn cycle assumptions. This investigation is motivated by the uncertainties of plasma physics involved in noninductive current drive and is an attempt to quantify the relative attractiveness of tokamak reactors operating with different burn cycles. By assessing each subsystem's reliability and lifetime under different operating circumstances we aim to quantify reactor performance characteristics. These results hopefully can serve as guidance in formulating future research and development efforts. This study is still in its early stages, so the results reported here are incomplete. Our present goal is mainly to elucidate the methodology of the analysis.

Five distinct operating modes have been identified for tokamak reactors: conventional Ohmically driven (OH); assisted noninductive startup (assisted OH); internal transformer (IT) which has no Ohmic drive capability; a (hybrid) scheme requiring alternate Ohmic and noninductive drives; and the steady-state (CW) typified by STARFIRE. The various reactor subsystems which are sensitive to differences in the operating modes include: first wall, limiter/divertor, breeder material and blanket structure, thermal energy conversion and storage, Ohmic heating coils, equilibrium field (EFC) coils, toroidal field (TFC) coils, electrical power supplies and energy storage, and noninductive driver systems. Figures of merit at the conclusion of our study will include capital cost trends, net electric output, and plant availability. We assume availabilities ≈80% will be mandatory for utility acceptance and will identify reactor design approaches and relative costs needed to meet this goal for the five different operating modes. Sensitivity to different assumptions will be shown.

The first question of interest is how high noninductive current drive efficiency must be to make CW operation a viable (economical) option. We can estimate upper limits on $\hat{j}/\hat{p}$. For high speed drivers ($v_\parallel/v_e > 1$) we see from Fig. 1 that $\hat{j}/\hat{p} \approx K\, v_\parallel^2/v_e^2$, with K ≈1-2, so j/p is independent of $T_e (= mv_e^2)$. In the relativistic limit the maximum value is achieved, $\hat{j}/\hat{p} \to 2\, c^2/v_e^2$, where c is the speed of light [4]. In this limit we have $j/p = 1.0 \times 10^{21}\, \bar{n}_e^{-1}$. We now assume a parabolic current density and relatively flat density profile and obtain $I_0/P_d^{(0)} = \gamma^{(0)}[7.0\ m/R_0]\bar{n}_{e20}^{-1}$ with $\gamma^{(0)}$ = 0.21 A/W. Next we solved the fusion power balance for a STARFIRE size reactor [R_0 = 7.0 m, A = 3.6, $\bar{\beta}_t$ = 0.067, q_ℓ = 2.5] over a range of operating temperatures $\bar{T}_e$. The toroidal magnetic field at the TFC was increased appropriately at the higher temperatures in order to keep fusion power (P_f = 4230 MW) and the wall load constant. While $\bar{n}_e$ varies inversely with $\bar{T}_e$, the equilibrium current, I_0, must increase with $\bar{T}_e$, due to the increasing values of B_M. The product $\bar{n}_e I_0$ has a minimum around $\bar{T}_e$ = 16 keV, so driver power $P_d^{(0)}$ is minimized at $\bar{T}_e$ = 16 keV. $P_d^{(0)}$ is shown in Fig. 7 for a variety of $\gamma^{(0)}$ values. In addition, the estimated net electric power production, $P_{net}^{(0)}$, is shown assuming a driver efficiency of η_d = 0.7.

Similar curves may be derived for low speed drivers ($v_f/v_e < 1$) for which $\hat{j}/\hat{p}$ has a maximum value [4,5] around 130 (for the CAW). In this case j/p is a function of T_e, and we obtain $I_0/P_d^{(1)} = \gamma^{(1)}[7.0\ m/R_0]\bar{T}_{e10}\bar{n}_{e20}$, with $\gamma^{(1)} = 0.16$ A/W for the CAW. Driver and net electric power are shown in Fig. 8 for various values of $\gamma^{(1)}$.

Several conclusions may be drawn from these curves. First, while P_{net} maximizes for $\bar{T}_e \gtrsim 12$ keV, the B_M value increases quite quickly at these higher temperatures. The difficulty of designing TF magnets with $B_M > 11$-12 T may be overwhelming. Secondly, it is not necessary to achieve $\gamma \gtrsim 0.1$ A/W in order to get large P_{net}. From the figures we note $P_{net} > 1000$ MW is possible for $\gamma \gtrsim 0.05$ A/W. Third, we see the driver capital cost may be the strongest motivation for achieving high efficiency. Evidently, $\gamma \gtrsim 0.3$ A/W is needed to reduce driver power sufficiently so that $P_d \lesssim 100$ MW. We note that unit costs exceeding \$1/watt have historically characterized high power systems, and it is probable that driver systems greatly exceeding ~\$1. $\times 10^8$ become economically untenable.

In our study of the four pulsed modes of operation we use simplified wave forms for duty cycles. Structural and system response and lifetime limitations will be characterized with respect to variations in the cycles, e.g. burn period length.

As one example of the work underway we present preliminary results regarding the sensitivity of one reactor subsystem to burn cycle variations. The structure of interest is the leading edge of the limiter. This component (see Fig. 9) has curved cooling channels of outer radius R = 7 mm; a structural heat sink of thickness 1.5 mm is coated with a material (beryllium in the present example) having plasma compatibility (benign sputtering characteristics). The coating thickness is determined in order to maximize the leading edge lifetime, and this lifetime dependence on surface heat flux and the number of fuison power cycles is computed.

First consider a copper heat sink with H_2O coolant at 130°C. For surface heating 0.75-1.75 MW/m^2, thermal stress associated with cyclic operation leads to fatigue failure of the copper in ~10^4-10^5 cycles if the beryllium coating exceeds ~4-16 mm in thickness. Reducing δ increases the fatigue life but reduces the number of disruptions the beryllium can stand before failure. The coating thickness is taken which results in equal cycle lifetimes due to both criteria. In a typical case where 140 μm is removed by a disruption, once in every 10^3 burn cycles, the fatigue curve for 1.75 MW/m^2 intersects the disruption curve at $N = 2.7 \times 10^4$ cycles with $\delta = 3.6$ mm. Now, from the point of view of radiation damage (swelling, ductility) copper is not a particularly attractive heat sink, its lifetime being on the order of two years in a reactor. Thus, in order for fatigue and disruptions to not be more limiting than radiation damage, we must demand burn periods long enough that $N = 2.7 \times 10^4$ cycles is not exceeded in two years of operation. This demands, for the example considered, a burn period $t_f > 1.8 \times 10^3$ s (at 80% availability). The dashed lines in Fig. 10 display the minimum burn periods for the copper limiter, assuming a two-year replacement period and with two values for disruption erosion.

A two-year life may be too short for a practical power reactor. Advanced materials may improve the situation. Therefore, we repeated our analysis for

a vanadium heat sink cooled by lithium at 210°C. Predictions for radiation damage in vanadium suggest integrated lifetimes of 24 MW-y/m^2 (neutron dose) are reasonable, resulting in replacement times on the order of six to twelve years. Thus, if such advanced alloys should become available there is an incentive to extend the burn period such that life is not limited to shorter times by cyclic effects. This is shown in the figure were t_f as long as $1. \times 10^4$ s may be desirable for a vanadium limiter and severe disruption damage.

We close this section with two observations. First, fatigue is not always a dominating concern for pulsed operation. In the example cited disruptions and radiation damage are very important. Thus, for this isolated example there is little motivation to achieve CW operation via noninductive current drive. The second observation is that other systems are expected to be more sensitive to pulsed operation. Of particular concern is fatigue associated with out-of-plane forces on the TFC structure, driven by the oscillating equilibrium (vertical) field associated with pulsed operation. Other important concerns are the higher costs of the electric power supplies and thermal energy storage needed for pulsed operation.

4. Conclusions

Table II summarizes the status of program needs for the four drivers presently of greatest interest. We emphasize that several options exist but that experimental studies need to be pursued for alternatives to the LH driver.

In the long run it seems necessary to test current drive in a long pulse tokamak capable of operation in excess of ~10^3 s. (Such a long pulse would doubtless also be useful for impurity generation monitoring and control attempts.) Such a tokamak would not need D-T fuel in order to address current drive questions, but auxiliary heating would be desirable in order to maintain reactor temperatures for long pulses. While resistive magnet designs may be capable of such long pulse operation, it would be worthwhile considering superconducting toroidal magnets. A superconducting tokamak would in principle permit true steady-state operation (many hours) and would require continuous power ($\gtrsim$10 MW) to maintain reactor temperatures, as well as to maintain the toroidal current.

Acknowledgments

I wish to thank D. Mikkelsen, C. F. F. Karney, and V. Bailey for their invaluable help in performing the DEMO calculations.

This work was supported by the U.S. Department of Energy.

References

[1] C. C. BAKER et al., Nucl. Eng. Design 63, (1981) 199.

[2] D. A. EHST et al., J. Fusion Energy 2 (1982) 83.

[3] M. Abdou et al., "Demonstration Tokamak Power Plant," in 12th Symp. on Fusion Technology, Jülich, FRG, Sept. 1982.

[4] M. ABDOU et al., Argonne National Laboratory, ANL/FPP/TM-154, (1982).

[5] N. J. FISCH and C. F. F. KARNEY, Phys. Fluids 24 (1981) 27.

[6] J. M. DAWSON and M. F. UMAN, Nucl. Fusion 5 (1965) 242.

[7] J. G. CORDEY et al, Culham Lab. Rep. CLM-P636 (1981).

[8] F. W. PERKINS, in "FED-A, An Advanced Performance FED Based on Low-q and Current Drive," [ORNL/FEDC-83/1], Y-K. M. Peng and P. H. Rutherford, eds. (1983).

[9] A. MOHRI et al., Proc. Conf. on Plasma Physics and Controlled Nuclear Fusion Research, 1978, Vol. III, p. 311 (IAEA, Vienna, 1979).

[10] A. MOHRI et al., Proc. Conf. on Plasma Physics and Controlled Nuclear Fusion Research, 1980, Vol. I, p. 511 (IAEA, Vienna, 1981).

[11] V. BAILEY et al., Physics international Co. Rep. PIFR-1466-1 (1982).

TABLE I

DEMO Current Driver Options

	Parallel Momentum Input	Indirect Means (Heating, Canonical Angular Momentum, etc.)
Particle injection driven currents	Neutral beam (NB) Partially ionized heavy atom beam Pulsed relativistic electron beam (REB) Pulsed intense (charge neutral) ion beam	Bootstrap Preferential alpha loss
Wave-driven currents	Compressional Alfven wave (CAW), $\omega \ll \Omega_i$ Shear Alfven wave, $\omega \ll \Omega_i$ Low-speed magnetosonic ($\omega \gg \Omega_i$) wave $\left.\begin{array}{l}\\ \\ \\ \end{array}\right\} \frac{\omega}{k_\parallel} < v_e$	Minority ICRH Alpha Landau and transit time damping
	Lower hybrid wave, Ion cyclotron wave, $\omega = \Omega_i$ High-speed magnetosonic (HSMS) wave $\left.\begin{array}{l}\\ \\ \\ \end{array}\right\} \frac{\omega}{k_\parallel} > v_e$	ECRH Anisotropic reflection of synchrotron radiation

TABLE II

Near-Term Current Drive Program in Support of DEMO for the Four Most Promising Driver Options

Driver	Theory/Calculation Needs	Experimental Tests[a]	Technology R & D
LH	Assess oscillating plasma scenario for reactors.	PLT/Alcator C: test linear theory, accessibility, resonance cones, frequency selection, $k_{\parallel}$ spectrum, density effects, etc.	High power cross-field amplifiers; radiation effects on waveguide windows; vacuum density control in waveguides.
FW	Ray tracing t $\omega/k_{\parallel} > 3\ v_e$ and $A \geq 5$; antenna coupling theory - spectrum for loops vs. phased reentrant waveguides.	PLT: Test electron TTMP, current drive; test reentrant waveguide performance.	Radiation effects on waveguide windows; design possibilities for antenna loops, recessed cavities, reentrant or ridged waveguides.
CAW	Effects of non-neoclassical electron orbits; phased antenna loop coupling, spectral theory; spatial damping, current density profile.	PLT/TEXT: study selective coupling to CAW; test electron TTMP, current drive; determine $k_{\parallel}$ spectral width.	Radiation effects on coax windows; design possibilities for antenna loops.
REB	Relativistic electron orbits, beam capture and penetration, resulting current density profile.	TEXT: test beam penetration, long pulse current density evolution; diode voltage, pulse width, current density, location, configuration relationships.	High voltage spark gaps; high energy density liquid dielectric capacitors; compulsators, rotating flux compressors; high voltage pulse transformers; radiation effects on coax windows; diode protection from disruptions.

[a] Device identified represents either ongoing experimental program or an indication of the type of device required to perform the experiments.

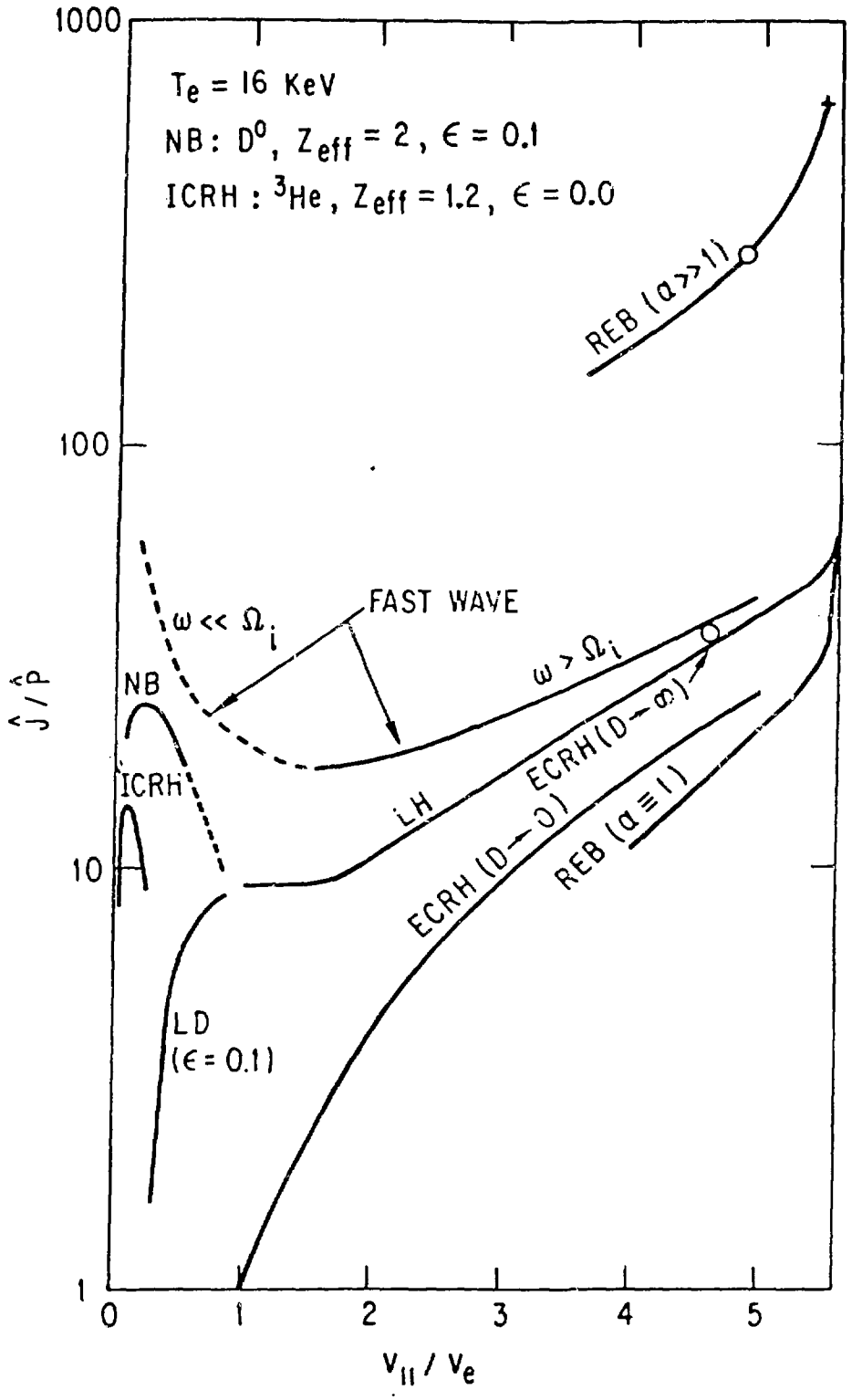

Fig. 1. Normalized current drive efficiency versus driver speed.

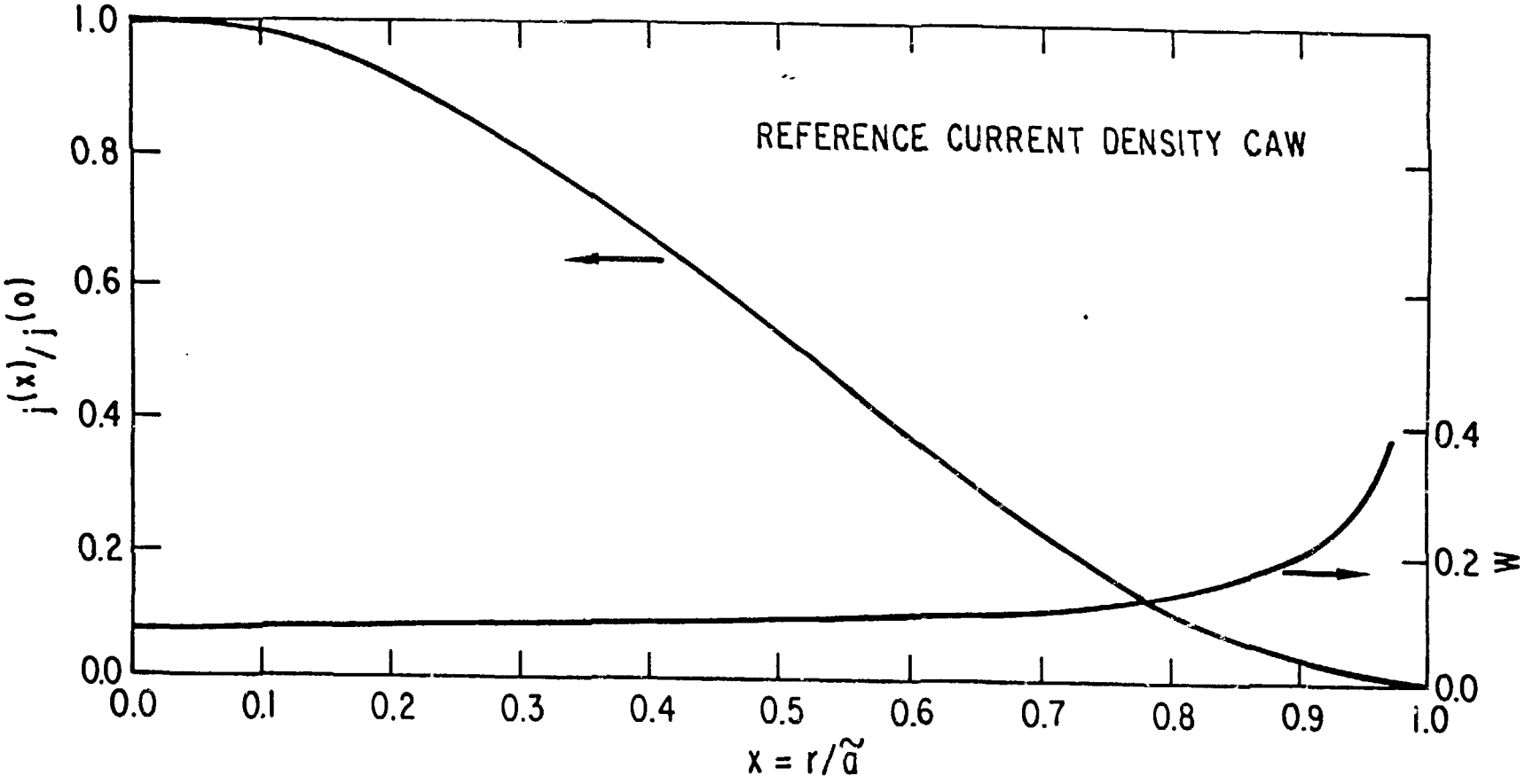

Fig. 2. Current density profile for compressional Alfven wave (5.3 MHz, $\lambda_{\parallel}$ = 1.6 m)

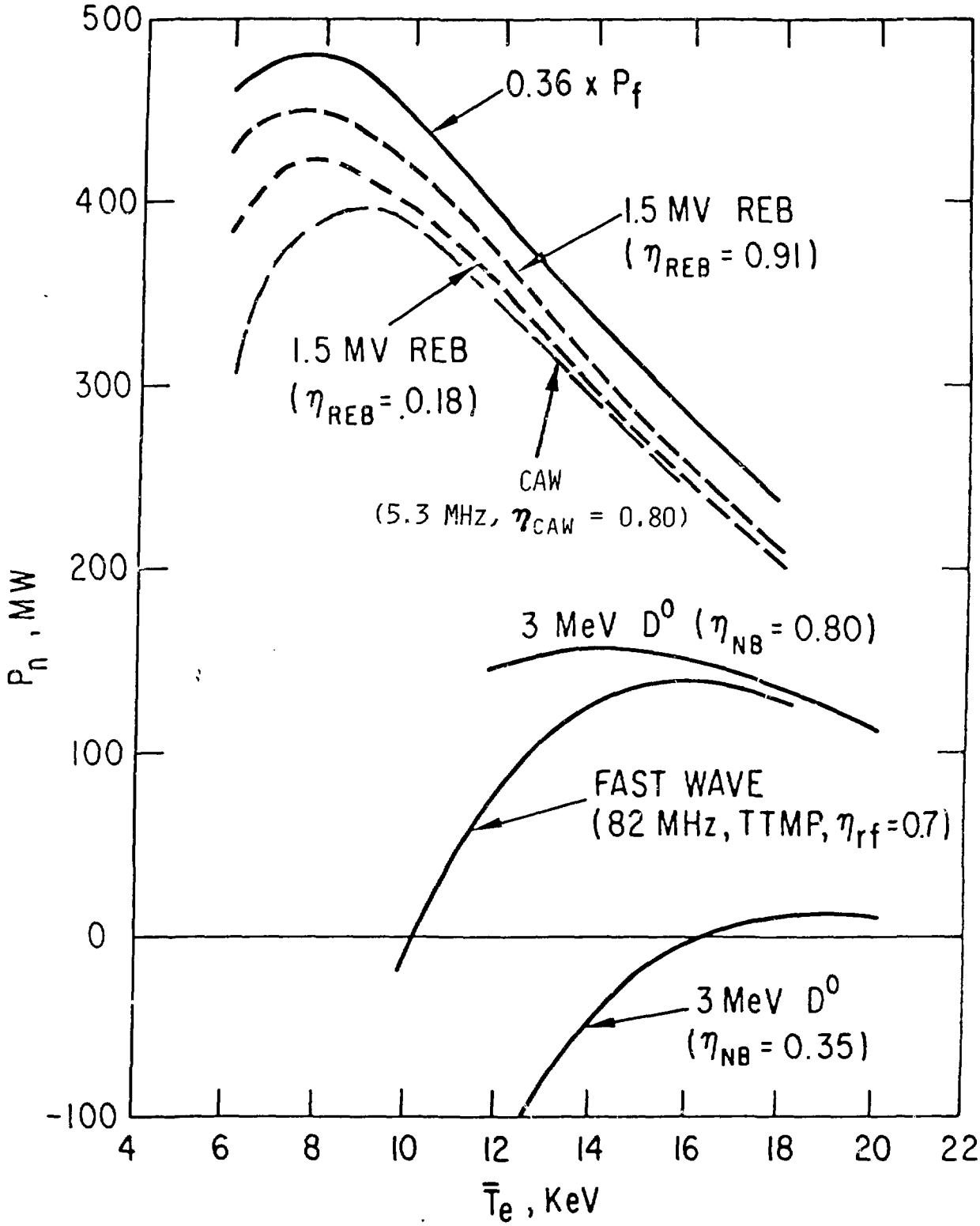

Fig. 3. Net electric power for DEMO with different current drivers.

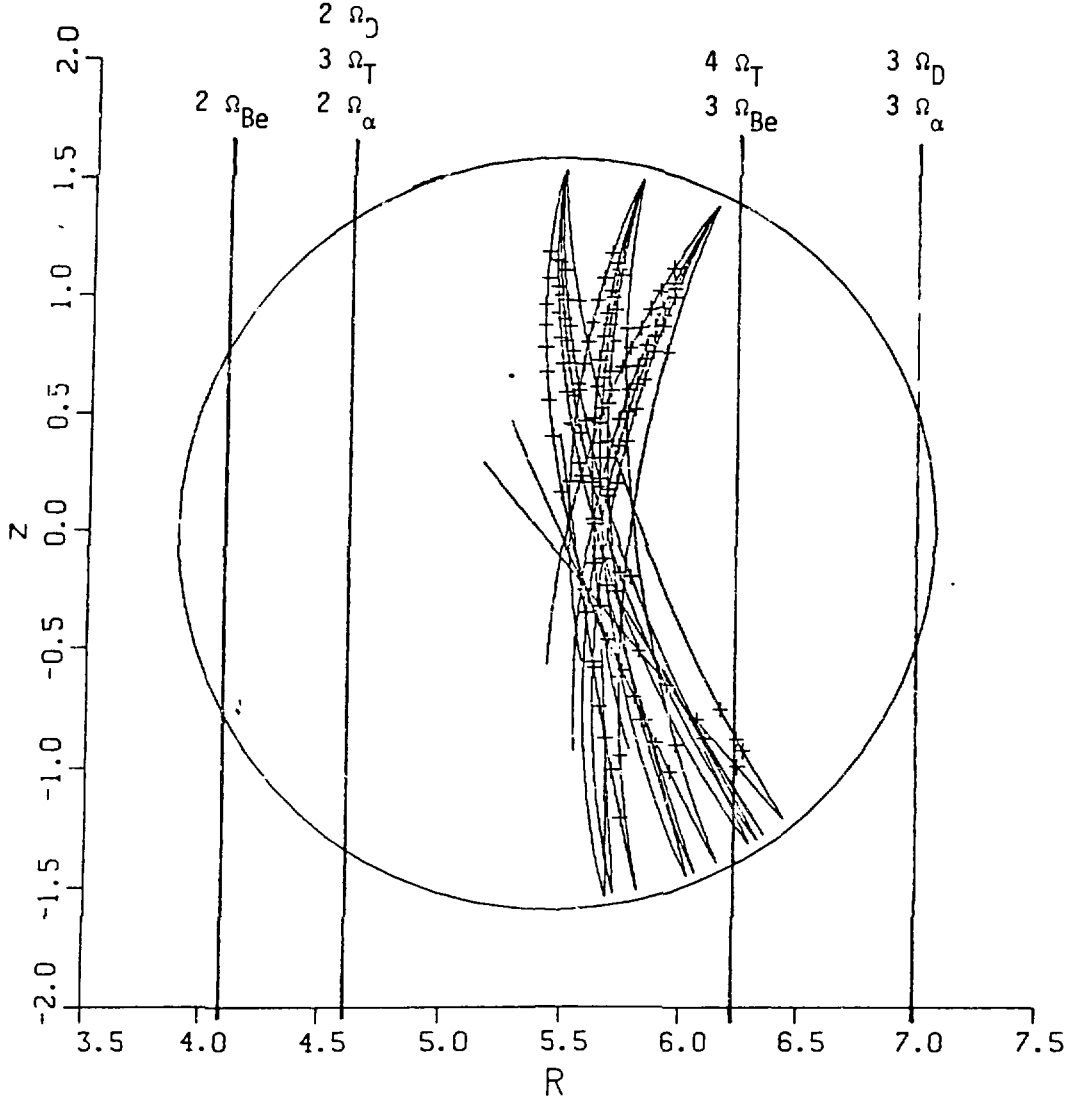

Fig. 4. Typical HSMS ray trajectories; $\bar{T}_e$ = 12 keV.

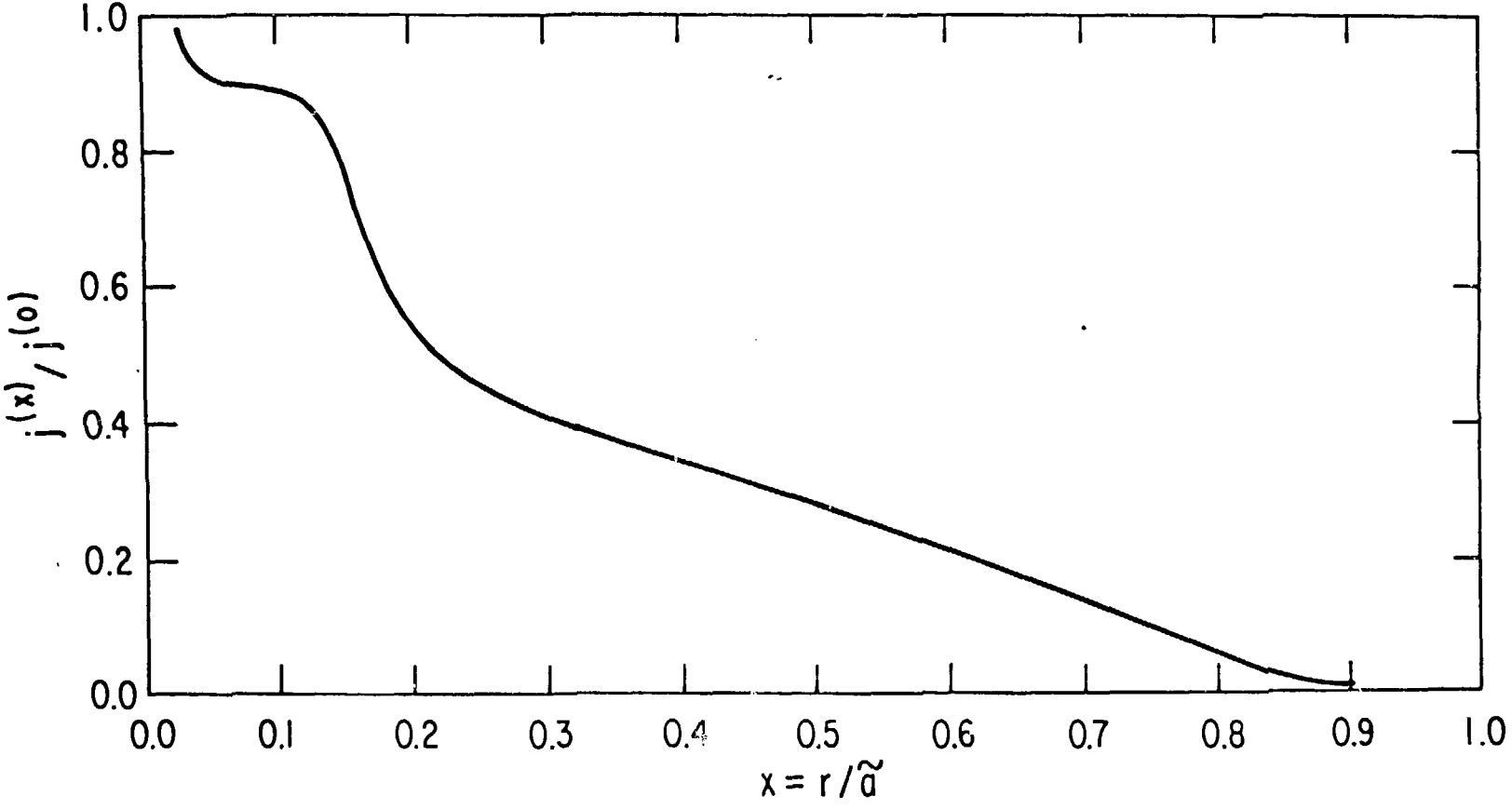

Fig. 5. Current density profile for HSMS at 82 MHz and $\lambda_{\parallel} \approx 0.8$ m; $\bar{T}_e = 16$ keV.

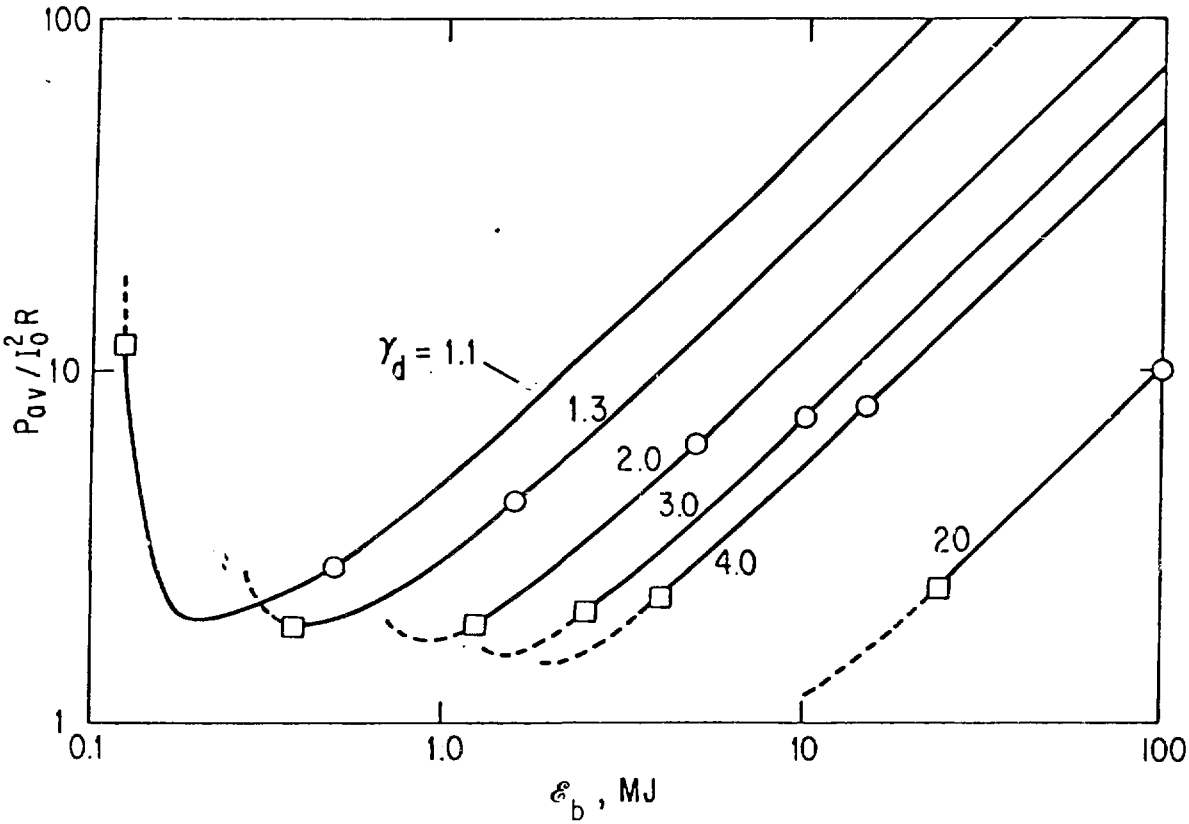

Fig. 6. DEMO with R_0 = 5.2 m, I_0 = 9.01 MA; analytic theory is valid between boxes and circles. Time average REB power is given in terms of relativistic γ_d at the diode and total beam kinetic energy, $\mathcal{E}_b$, in the pulse.

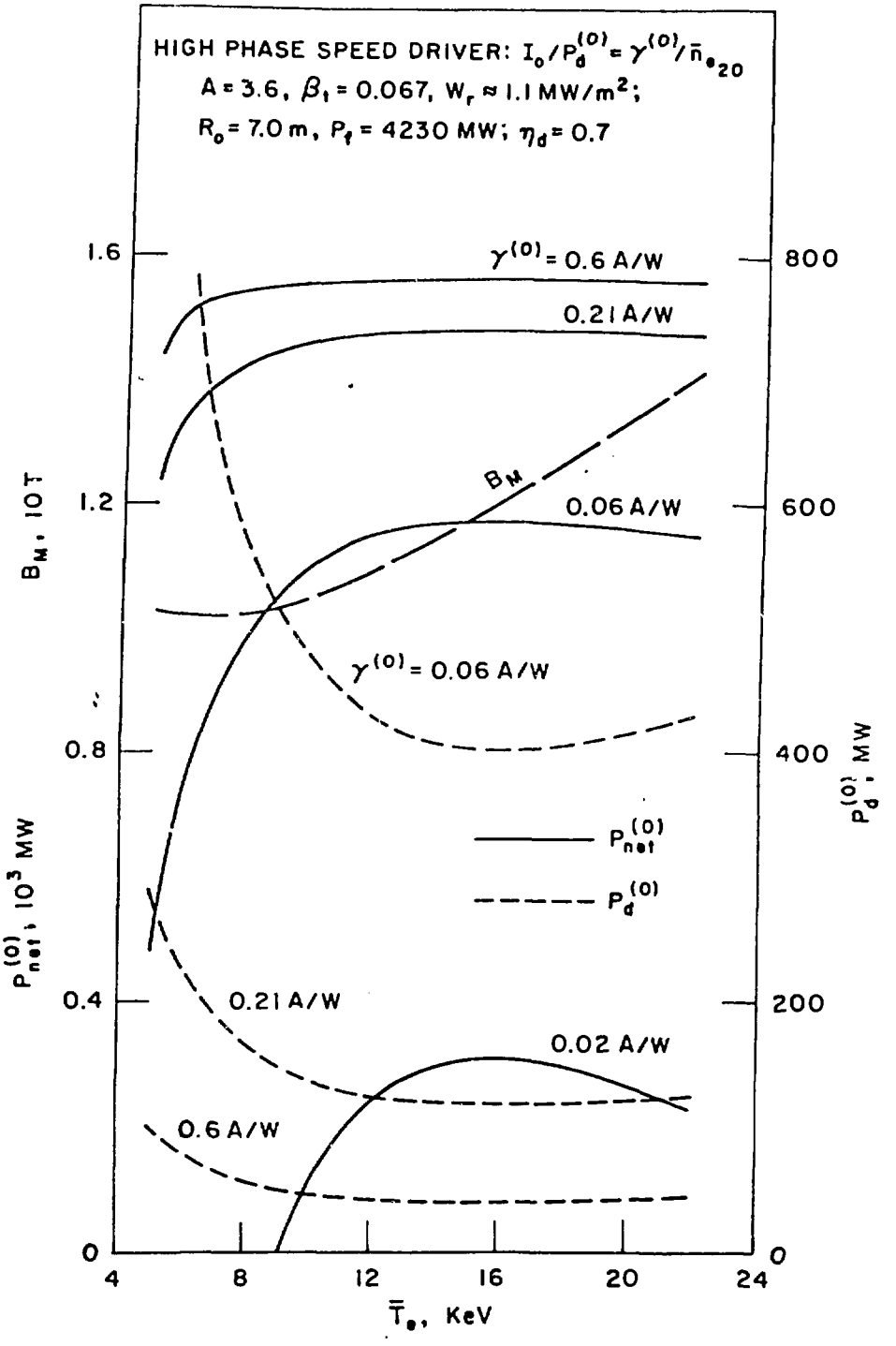

Fig. 7. Driver power and reactor net power for high speed driver ($v_f > v_e$) and various efficiency coefficients.

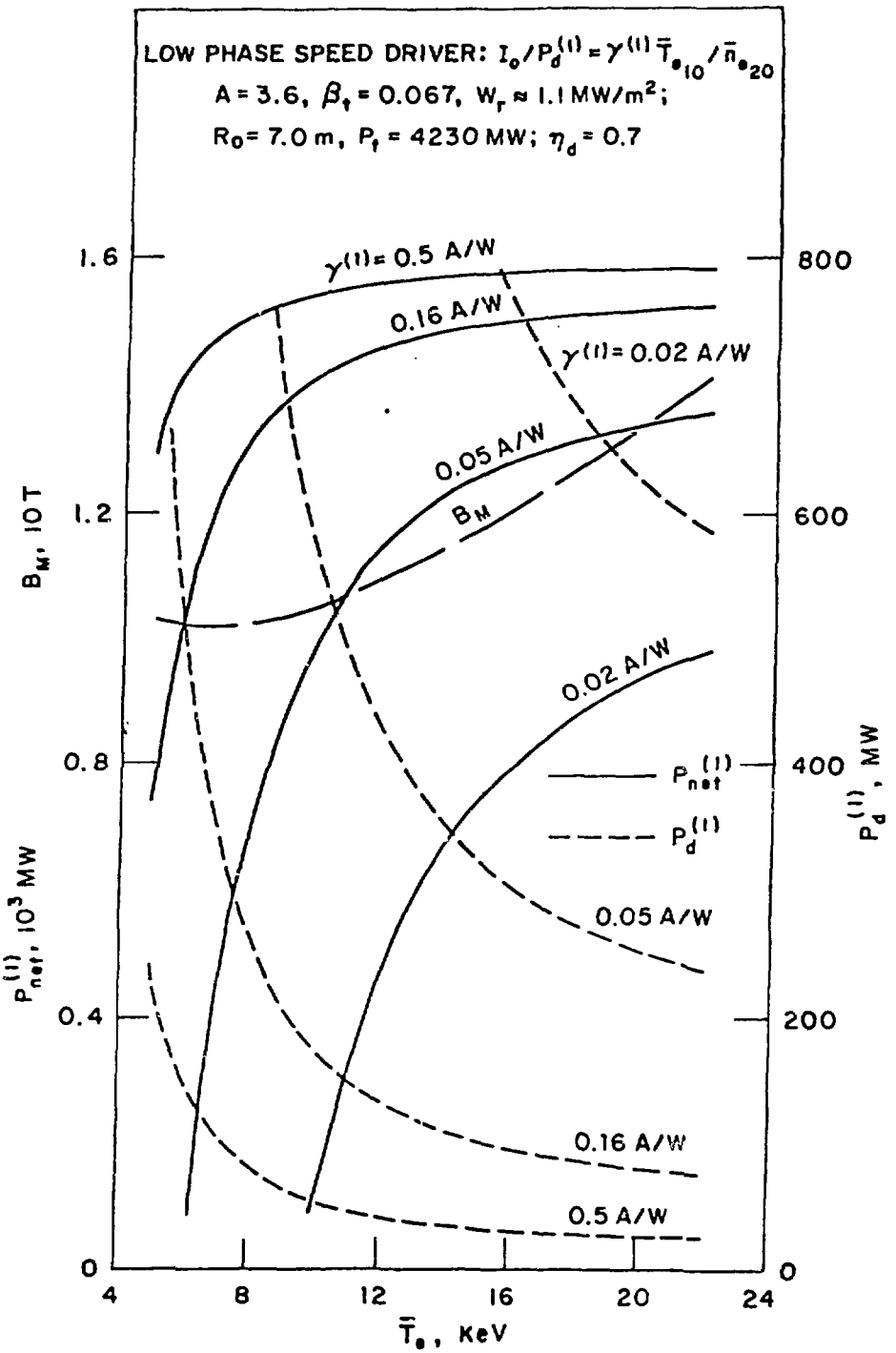

Fig. 8. Driver power and reactor net power for low speed driver ($v_f < v_e$) and various efficiency coefficients.

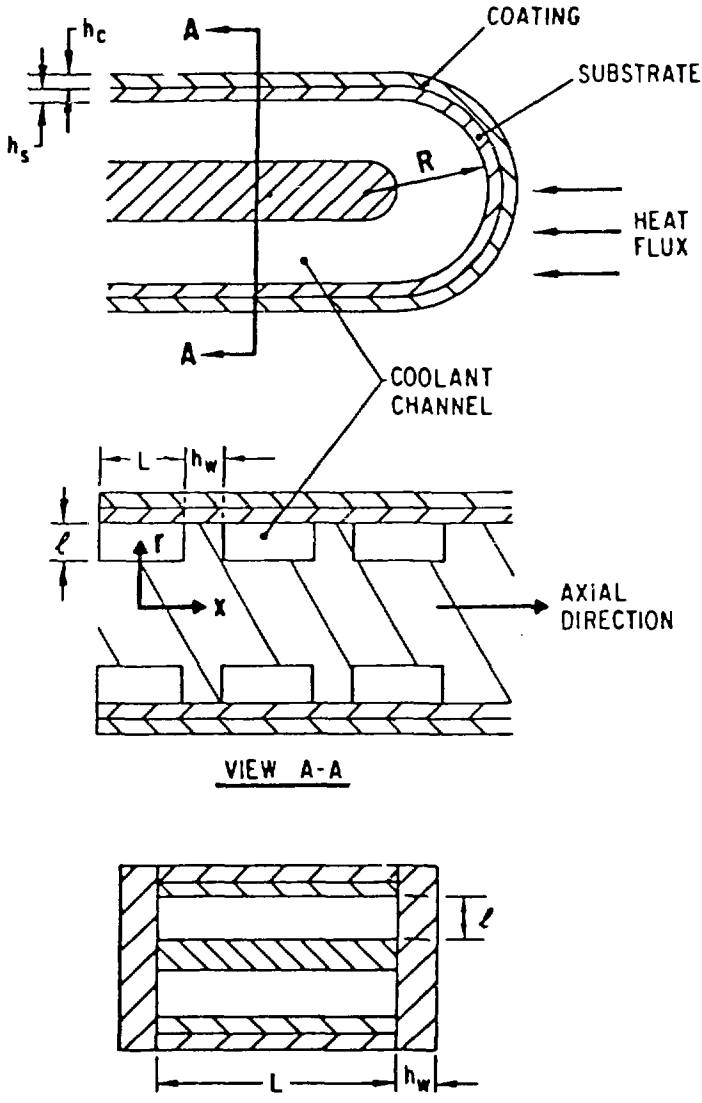

Fig. 9. Leading edge geometry used for stress calculations in limiter; INTOR model.

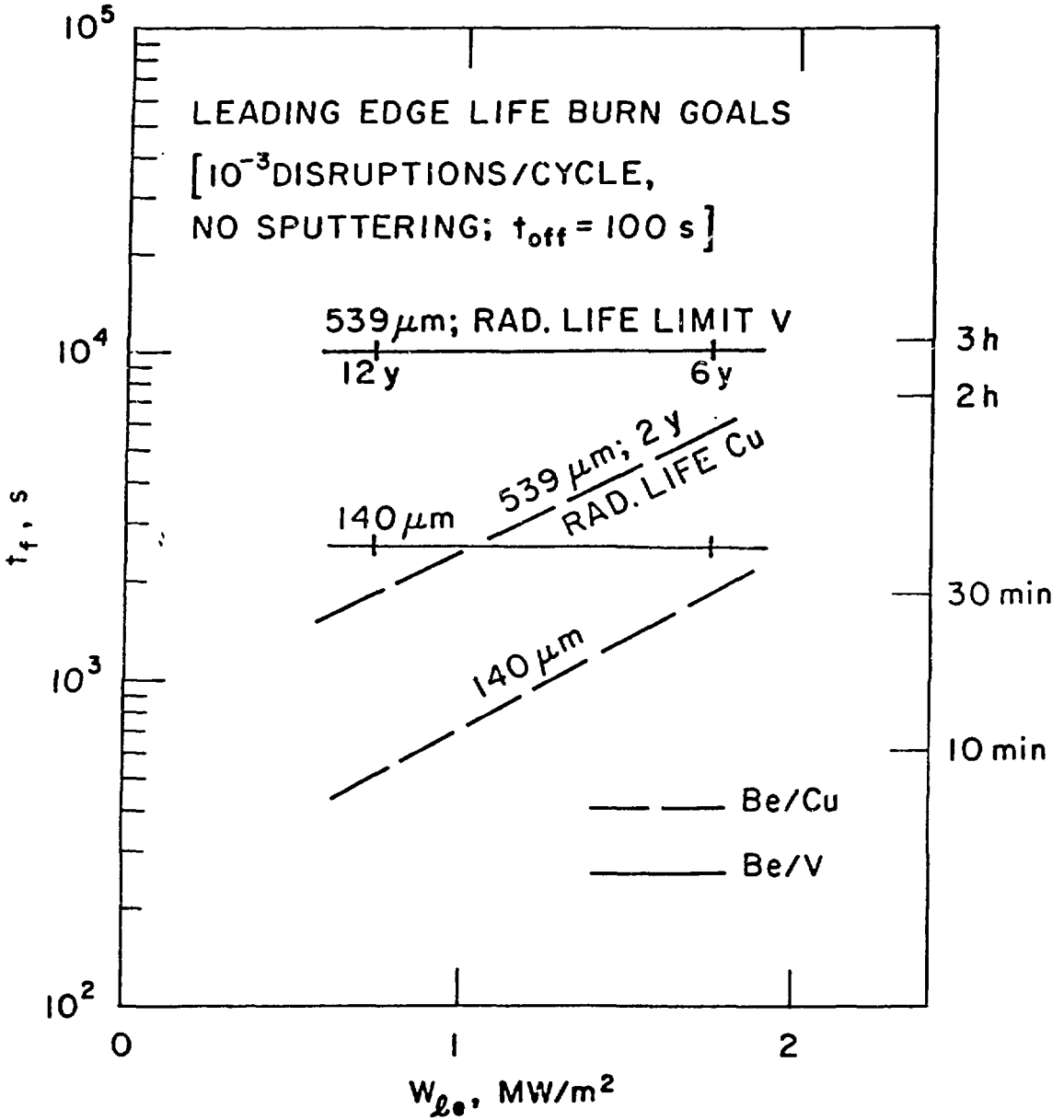

Fig. 10. Minimum burn periods required such that cyclic effects (from thermal fatigue and disruption damage) are less life limiting than radiation damage. Disruption damage is parameterized by moderate (140 μm) and severe (539 μm) beryllium losses per disruption.